MDPI

Review
Recent Achievements of the ERNA Collaboration

Raffaele Buompane [1,2,*], Antonino Di Leva [2,3], Lucio Gialanella [1,2], Gianluca Imbriani [2,3], Lizeth Morales-Gallegos [1,2] and Mauro Romoli [2]

1 Dipartimento di Matematica e Fisica, Università della Campania "L. Vanvitelli", Viale Lincoln, 5, 81100 Caserta, Italy; lucio.gialanella@unicampania.it (L.G.); moralesgallegos@na.infn.it (L.M.-G.)
2 Istituto Nazionale di Fisica Nucleare, Sezione di Napoli, Via Cintia snc, 80126 Napoli, Italy; dileva@na.infn.it (A.D.L.); imbriani@na.infn.it (G.I.); romoli@na.infn.it (M.R.)
3 Dipartimento di Fisica "E. Pancini", Università di Napoli "Federico II", Via Cintia snc, 80126 Napoli, Italy
* Correspondence: raffaele.buompane@unicampania.it

Abstract: For more than two decades, the ERNA collaboration has investigated nuclear processes of astrophysical interest through the direct measurement of cross sections or the identification of the nucleosynthesis effects. Measurements of cross-section, reported in this publication, of radiative capture reactions have been mainly conducted using the ERNA Recoil Mass Separator, and more recently with an array of charged particle detector telescopes designed for nuclear astrophysics measurements. Some results achieved with ERNA will be reviewed, with a focus on the results most relevant for nucleosynthesis in AGB and advanced burning phases.

Keywords: nuclear astrophysics; recoil mass separator; charge particle spectroscopy; carbon burning

1. Introduction

Radiative capture reactions involving hydrogen or helium are of key importance for stellar evolution and nucleosynthesis when the latter occurs in massive stars [1]. The large majority of the direct experimental information on radiative capture reactions has been collected measuring the reaction yields through the observation of the emitted γ-rays [2,3]. While γ-ray spectroscopy offers several advantages, when measuring the extremely low cross sections that characterize nuclear processes of astrophysical interest, it encounters severe limitations owing to the various backgrounds due to cosmic rays, natural radioactivity, and beam-induced parasitic reactions. As an alternative, the direct detection of the nuclei produced in the reaction is being exploited since a few decades. This can be achieved, at the cost of a significant technical complication, using a recoil mass separator (RMS).

The European Recoil Separator for Nuclear Astrophysics (ERNA) is a RMS designed with the main goal of determining the $^{12}C(\alpha, \gamma)^{16}O$ reaction cross-section, with the effort of the collaboration bearing the same name since 1998. The ERNA Collaboration studied several processes with the RMS, with charged particle spectroscopy, and also ran other experiments [4–10].

In addition, conventional and accelerator mass spectroscopy have been exploited to study materials of astrophysical interest.

Some of the main results achieved on cross-section measurements, with a focus on the ones most relevant for AGB star nucleosynthesis and advanced nuclear burning stages, will be reviewed.

2. Materials and Methods

Over the years, the ERNA Collaboration studied several reactions with the namesake RMS. More recently, the collaboration developed an array of two layer charged particle detectors, named GASTLY (GAs Silicon Two-Layer sYstem), especially tailored to the measurement of the $^{12}C+^{12}C$ reaction processes with the thick target approach.

The RMS and the related experimental method are introduced in the next subsection, while the GASTLY array and the thick target approach are presented in the following one.

2.1. Recoil Mass Separator ERNA

The direct detection of the recoiling nuclei produced in the fusion process is the goal of the RMS approach.

In a radiative capture reaction, the fusion of projectile and target particles produces a nucleus that recoils in the laboratory frame system with a momentum quite similar to the one of the projectile [11]. In fact, at a given center of mass energy, the emission of the γ-ray introduces a change in momentum that depends on the emission angle and the Q-value of the reaction. Thus the nuclei produced in the fusion process (in the laboratory frame) will emerge from the interaction within a cone of maximum opening $\vartheta_{\max}$ with respect to the direction of the projectile. This means that the secondary beam composed by the recoils will be diverging right after the target and needs to be focused toward the beam axis to be efficiently transported further. It is advantageous to keep $\vartheta_{\max}$ as small as possible; therefore, the reaction is usually studied in inverse kinematics. In such conditions, the recoils emerge from the target together with the primary beam with a typical ratio of $10^{-10} \div 10^{-17}$ or lower, depending on the cross-section under study. In order to count the recoils in a detector, most of the primary beam particles need to be filtered out. Therefore, an RMS consists of a series of filters and focusing elements that allows for an efficient suppression of the primary beam and ensures the transport of all recoils (in a given charge state) at the end detector such that they can be identified and counted.

The number of recoils N_r observed in the final detector, having an efficiency ϵ, is given by [1]

$$N_r = N_b \cdot T_{RMS} \cdot \Phi_{q_r} \cdot \epsilon \cdot \int_{E_b - \Delta E_b}^{E_b} \frac{\sigma(E)}{|dE/dN_t|} dE \ , \tag{1}$$

where N_b and $T_{RMS}(q)$ are, respectively, the number of projectiles impinging on the target and the transmission of the recoils from the target to the final detector, when the recoil charge state q_r with probability Φ_{q_r} is selected.

The interaction cross-section $\sigma(E)$ is integrated over the beam energy loss in the target ΔE_b at the beam energy E_b that is determined by the stopping power of the beam ions in the target dE/dN_t, where N_t is the number of nuclei per unit target area. Of course, an accurate and precise determination of $\sigma(E)$ relies on an adequate estimate of all quantities in Equation (1).

To obtain results that are as much as possible independent from the usually unknown distribution of the recoils in the phase space $(\vec{r},\vec{r}')$ (position, velocity), it is necessary to fulfill the condition $T_{RMS}(q) = 1$. The most effective method to know in detail the acceptance of the separator, i.e., the capability of the RMS to transport to the end detector the recoils regardless of their angle and energy, is to directly measure it. This can be done using a pilot beam mimicking the recoils beam properties, that can be achieved with an electrostatic deflection unit, and varying the beam energy to sample the emittance of the recoils and determine their transmission through the RMS, as reported in [4,12].

The recoil mass separator ERNA is one of the few recoils separators devoted to the measurement of nuclear cross section of astrophysical interest. The first RMS of this small group was built at Caltech, although the limited beam suppression imposed to detect recoils in a coincidence with capture γ-rays in NaI detectors at the target position. Later, the NABONA Collaboration (NAples BOchum Nuclear Astrophysics) built and commissioned a RMS devoted to the measurement of the ^{7}Be(p, γ)^{8}B cross-section relying only on recoils detection, using a windowless hydrogen gas target and a ^{7}Be beam [13]. Building upon this successful experience, the same groups started a new project to realize the ERNA RMS at the 4MV Dynamitron Tandem Laboratorium of the Ruhr-Universität Bochum (Germany) [12,14–17], with the aim of studying the ^{12}C(α, γ)^{16}O reaction [18].

During the same years, the Daresbury Recoil Separator, previously used for nuclear structure studies, found a new home at the Holifield Radioactive Ion Beam Facility at the Oak Ridge National Laboratory (USA) [19]. The DRAGON (Detector of Recoils And Gammas Of Nuclear reactions) RMS was built and commissioned at TRIUMF in Vancouver (Canada) [20]. The ARES (Astrophysics REcoil Separator) RMS at the Cyclotron Research Center in Louvain-la-Neuve (Belgium) [21] was used for a few measurements. An RMS devoted to the study of the $^{12}C(\alpha, \gamma)^{16}O$ was assembled at the Kyushu University Tandem Accelerator Laboratory (Japan) [22].

More recently, the commissioning of two new RMS, the St. George at the Nuclear Science Laboratory of the University of Notre Dame (USA) [23] and the SECAR (SEparator for CApture Reactions) at the National Superconducting Cyclotron Laboratory and Facility for Rare Isotope Beams (FRIB) at Michigan State University (USA) [24], were completed. Few other RMSs are in different stages from design to commissioning.

In 2009, ERNA was moved to the Tandem Accelerator Laboratory of the CIRCE (Center for Isotopic Research on Cultural and Environmental heritage), University of Campania—INNOVA, Caserta, Italy, where a 3.0 MV NEC 9SDH-2 Pelletron accelerator is located [25]. This has provided the opportunity for an upgrade in the separator's layout. In particular, a further momentum filtering element, the Charge State Selection Magnet (CSSM in the following), has been placed after the gas target and before the first focusing element of the separator. The layout of the separator at CIRCE is shown in Figure 1.
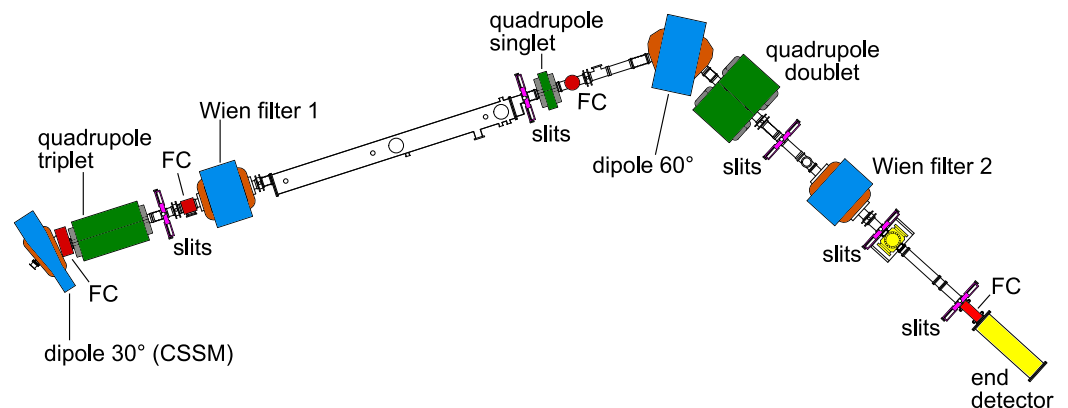

Figure 1. Layout of the ERNA RMS at the CIRCE Tandem Accelerator Laboratory. CSSM indicates the charge state selection magnet; FC indicates the Faraday cups along the separator.

The CIRCE Tandem Accelerator is equipped with two 40-sample MC-SNICS (Multi-cathode source of Negative Ions by Cesium Sputtering) Cs-sputter negative ion sources. One is used for the production of stable species ion beams and AMS (accelerator mass spectrometry) measurements. A second one is dedicated to the production of offline radioactive ion (RI) beams, in particular ^{7}Be [26,27]. This has offered the opportunity to investigate processes with both stable and RI beams.

Following the sources, the ions are analyzed by a 45° spherical electrostatic analyzer sector and a 90° double focusing bending magnet. Then, the beam is focused by an einzel lens and injected in the Pelletron accelerator toward the terminal. Here, the tandem is equipped with an Ar gas stripper with the aim to change the negative charge state injected at low energy in a positive one. The positive ions at the high energy end of the accelerator are focused by an electrostatic quadrupole triplet and analyzed by the double focusing 90° analyzing magnet and two 45° electrostatic spherical analyzers. The coupled action of these high-energy analysis stages ensures to a high degree that no contamination having the same mass of the recoils is present in the primary beam. The beam transport is assisted by a diagnostic based on Faraday cups (FC) and beam profile monitors.

The projectiles are then guided into the ERNA beam line by the switching magnet that is followed by a magnetic quadrupole triplet used to focus the beam onto the gas target.

A set of magnetic steerers is used for fine-tuning of beam position and direction toward the target in both horizontal and vertical plane in order to meet the stringent requirements needed for an efficient transport of the recoils through ERNA, in particular, a small angle, $\lesssim 0.2$ mrad, with respect to the beam axis.

Depending on the reaction under study, the separator has been provided with different windowless gas targets: extended ^{4}He and ^{3}He target for the study of the ^{12}C$(\alpha, \gamma)^{16}$O and ^{3}He$(\alpha, \gamma)^7$Be, respectively [4,17], another different extended ^{4}He one for the study of ^{15}N$(\alpha, \gamma)^{19}$F [5], an extended H$_2$ target for the measurement of the ^{7}Be$(p, \gamma)^8$B cross-section [28], and a supersonic jet ^{4}He one [29] in view of the measurement of the ^{12}C$(\alpha, \gamma)^{16}$O at even lower energies. The gas targets are provided with an additional Ar gas layer (post-stripper) so that recoils reach charge state equilibrium regardless of the reaction position within the target.

As said, an RMS is an alternating series of filters and focusing elements. The first filtering element of ERNA is the CSSM placed at the shortest distance allowed by geometrical constraints from the target, about 42 cm away. Its role is to select a single charge state for both projectile and recoil ions before the actual mass separation takes place. The next filtering element is the first velocity filter (Wien filter 1) that removes most of the primary beam thanks to the fact that projectiles and recoils have similar momenta and thus different velocities. The other filters are the 60° dipole magnet and the second velocity filter (Wien filter 2) that suppress the part of the primary beam that for different reasons may pass Wien filter 1, e.g., scattering in the target area. The recoils beam focusing is provided by the magnetic quadrupole triplet, the quadrupole singlet, and the quadrupole doublet. Several FCs, slit systems, apertures, and a magnetic steerer (not shown in Figure 1) are installed along the RMS beam line for setting-up and diagnosis purposes.

ERNA is fully computer-controlled, which allows simple operation and ensures long-term stability.

2.2. Charged Particle Spectroscopy

A dedicated beamline for the study of nuclear reactions relevant for astrophysics with charged particle spectroscopy was installed in 2014 at the CIRCE accelerator laboratory within the framework of the ERNA Collaboration.

For this purpose, an array of ΔE-E_{res} detectors called GASTLY has been developed. Each GASTLY module houses in an aluminium pyramidal case, a detector telescope consisting of an ionization chamber (IC) for the ΔE signal, and immediately behind the IC, a large area silicon strip detector (SSD) acting as the E_{res}.

The IC is composed by a square section truncated pyramid fiberglass frame, whose cathode also acts as the module entrance window (23.0×23.0 mm^2, 2.6 μm thick Havar), a Frisch grid, an anode, and several guard rings. A schematic view of an individual GASTLY module is shown in Figure 2. The IC is filled with a suitable gas (typically CF$_4$) maintained at an appropriate pressure, chosen between 35 and 300 mbar according to the energy of the particles to be detected. The choice of an IC as ΔE detector, whose effective thickness and dead layers materials can be adapted to different experimental requirements, allows a high versatility, a long life, and an overall low cost of the system. The SSD has an active area of 58×58 mm^2 and is 300 μm thick. The front is segmented in 16 strips that can be read individually, providing good angular resolution capabilities and an improved energy resolution to the detectors. Despite the small signals outcoming from the IC, the use of homemade low-noise preamplifiers [30] placed inside the aluminium case for both the IC and SSD signals allows us to obtain an excellent noise to signal ratio and, consequently, a satisfactory particle identification, as shown in Section 3.2.
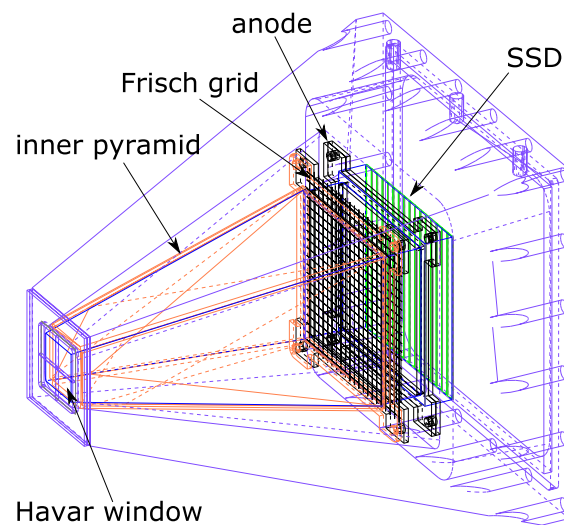
Figure 2. Wireframe view of a GASTLY module showing all the major components: the aluminium housing, the Havar entrance window acting as the cathode of the IC section that is defined by the inner fiberglass pyramid, the Frisch grid, the anode, and the SSD.

In order to cover a solid angle as large as possible, the GASTLY detector array was designed so as to allow for up to eight individual modules to be arranged around the beam axis. Thanks to its modularity and flexible configuration, the GASTLY array can be used in the backward and forward hemispheres. This allows to perform experiments using thick and thin targets and, depending on the target and detectors position, allows for the possibility of measuring angular distributions both at forward and backward angles.

For the study of the ^{12}C+^{12}C fusion process, the method preferred is the thick target approach that is briefly described in the following.

In order to use intense beams and avoid the issues related to target deterioration, thick targets can be used—in this case, highly ordered pyrolitic graphite (HOPG) 1 mm thick. However, other technical difficulties have to be faced, e.g., target temperature stabilization, radiated heat, detectors cooling, deposition of sputtered carbon, etc., all efficiently afforded with the GASTLY array, see [30,31] for further details.

Using an infinitely thick target, the measured yield $Y^\infty(E_b)$ corresponds to the integral of the cross-section from beam energy to zero. From the point of view of the measured yield, the number of events N counted in a peak corresponding to a particle group the thick-target yields Y^∞ are calculated, at each beam energy E_b, as [1] :

$$Y^\infty(E_b) = \frac{N\,q\,e}{\eta\,Q}, \tag{2}$$

where q is the charge state of the beam and e is the elementary charge; Q is the total charge collected on target during beam irradiation; and η refers to the detection efficiency.

To arrive at a thin-target yield $Y(E_b)$ and to extract the cross section, the thick-target yield is differentiated, i.e., $Y(E_b)$ is obtained, provided that the energy step size Δ is small compared to the width of any resonance structure possibly present in the energy range under consideration, from the difference between two adjacent points $Y^\infty(E_b)$ and $Y^\infty(E_b - \Delta)$; see, e.g., [32,33] for details.

3. Results

The ERNA RMS so far has provided data on several processes of astrophysical relevance. The first results were from the measurement of the total cross-section of the ^{12}C$(\alpha, \gamma)^{16}$O reaction [34]. This measurement significantly extended the energy range of the measurements available at that time with a considerable improvement on the overall

precision. It was possible to get a new insight on the relevance of the cascade transitions that were later investigated by DRAGON [35] and ERNA [36].

The use of ERNA RMS for the measurement of the ^{3}He$(\alpha, \gamma)^7$Be reaction cross-section led also to relevant results. Besides giving an important contribution to solve the then long-standing issue of the difference between extrapolation based on experiments selected according to the measurement method, the results indicated that at energies above $E_{\text{c.m.}} \simeq 1$ MeV the energy dependence was significantly different from the one foreseen by the most adopted models. This has lead to a selection of the available models that in turn corresponds to more robust extrapolations to stellar energies [4].

More recently, the ERNA Collaboration completed the measurement of the ^{7}Be$(p,\gamma)^8$B total cross-section in the energy range E_{eff} = 367.2 keV to 812.2 keV using the radioactive ^{7}Be beam available at CIRCE with intensities up to 10^9 pps [27]. For the first time, a measurement performed using the inverse kinematics approach, provides results with adequate precision to determine the cross-section of ^{7}Be$(p,\gamma)^8$B at astrophysical energy. The experimental apparatus has been described in detail in [28,37]. The zero-energy extrapolated astrophysical factor measured yields $S_{17}(0) = 16.6 \pm 2.1$ eV b. This value is compatible only with a part of previous measurements that yields lower value of $S_{17}(0)$, thus strengthening the discrepancy between existing data sets. A detailed description of the data analysis is presented in [9] and its supplemental material.

The results most relevant for AGB nucleosynthesis are discussed in more detail below.

3.1. Measurement of the ^{15}N$(\alpha, \gamma)^{19}$F Reaction Cross Section

The origin of ^{19}F has been widely discussed in recent years; see, e.g., ([38] and references therein). It is widely recognized that AGB stars contribute to the galactic fluorine production [39], and a direct evidence are the spectroscopic observations of [F/Fe] enhancements in low-mass AGB stars ([40] and references therein). Other possible production sites, implying higher temperatures, are core-collapse supernovae (SN) [41] and Wolf–Rayet stars [42]. In AGB stars, at temperatures of ~ 100 MK, the most direct production process is the ^{15}N$(\alpha, \gamma)^{19}$F reaction, although a nontrivial reaction chain is required to build a sufficient ^{15}N abundance. In fact, at the end of hydrogen burning, the ^{15}N is almost completely destroyed by the efficient proton capture reaction, while ^{14}N is relatively abundant. As it is known in low-mass AGB stars, the ^{13}C$(\alpha, n)^{16}$O is an efficient source of neutrons that can eventually lead to the reaction chain [39,43,44]

$$^{14}\text{N}(n, p)^{14}\text{C}(\alpha, \gamma)^{18}\text{O}(p, \alpha)^{15}\text{N}(\alpha, \gamma)^{19}\text{F} \ .$$
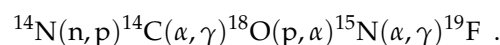
The AGB temperatures vary between 20 to 120 MK depending on the star's mass. At these temperatures, the reaction rate of the ^{15}N$(\alpha, \gamma)^{19}$F is determined by a number of narrow resonances, the most important being the $E_{\text{c.m.}}$ = 364 keV one, with some contribution from the $E_{\text{c.m.}}$ = 536 and 542 keV resonances. The direct capture (DC) component and the tails of the two broad resonances at $E_{\text{c.m.}}$ = 1323 and 1487 keV also play a major role at the lowest temperatures; see, e.g., [38] for a detailed discussion.

Before ERNA measurements, the most comprehensive work was performed by Wilmes et al. [45]. In this work, all the resonance strengths in the energy window 0.6 to 2.7 MeV were measured. The earlier works of Rogers et al. [46] and Price [47] also provide relevant information on resonances parameters.

In addition, the strength of the 364 keV resonance has been determined through an indirect measurement by de Oliveira et al. [48] using the ^{15}N$(^7$Li, $t)^{19}$F reaction at 28 MeV. Owing to the approximations needed in the model to derive the results, an uncertainty of factor of 2 is assumed.

The ERNA RMS was used to measure the reaction yield of the resonances at $E_{\text{c.m.}}$ = 1323 and 1487 keV. The reaction was studied in inverse kinematics, using a ^{15}N beam on a windowless extended ^{4}He target. For this purpose, enhanced intensity of N beam from a SNICS source was thoroughly investigated [49]. A sample ΔE-E_{res} spectrum is shown in Figure 3.

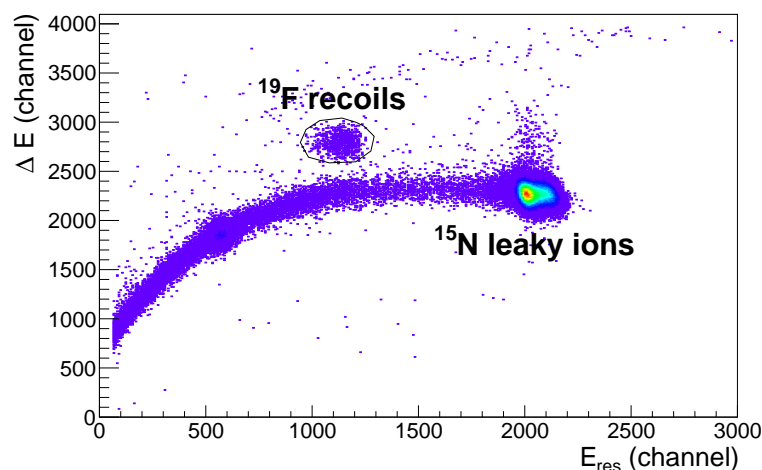**Figure 3.** Identification of the fluorine recoils produced in the $^{15}N(\alpha, \gamma)^{19}F$ reaction with the ICT (ionization chamber telescope).

The ^{19}F recoils are clearly identified, although ^{15}N leaky ions from the primary beam also reach the final detector. The yield of the two resonances was observed as a function of the energy, from well below the nominal resonance energy until the resonance energy was not reached within the target due to the energy loss in the extended target. Thus, from the convolution of the cross-section expressed as a Breit–Wigner function and the target density profile, the widths Γ_γ and Γ_α could be extracted for both resonances. A detailed description of the analysis is given in [5].

The astrophysical consequences of the measurements result are discussed in the next Section.

3.2. Measurement of the $^{12}C+^{12}C$ Fusion Processes Cross Section

Carbon fusion reactions are responsible of the fate of massive stars and the properties of a star right before a SN explosion. The value of the reaction rate, together with a complex interplay with electron degeneracy, neutrino cooling and the second dredge up, determine the minimum mass that the star's C-O core has to have to undergo C burning. If C is ignited, the $^{12}C+^{12}C$ reaction also determines whether or not the core will attain the Chandrasekhar mass limit. If so, the further burning stages will be entered and eventually the star explodes as a core-collapse SN, otherwise the star will end its life as an electron capture SN. Carbon fusion reactions are also essential to model X-ray bursts and explosions on the surface of neutron stars ([50,51] and references therein).

The present understanding of carbon burning requires the $^{12}C+^{12}C$ reaction rate to be known down to $E_{c.m.} = 1.5 \pm 0.3$ MeV [52]. At these energies, the $^{12}C+^{12}C$ reactions proceed mainly through the $^{23}Na+p$ and $^{20}Ne+\alpha$ channels. The corresponding cross-sections are extremely small, $\ll 10^{-9}$ b, and thus quite complex to be directly measured in the laboratory [53,54]. The extrapolation to astrophysical energies is made difficult by the presence in the measured data of several resonant structures ([55] and references therein) and a still unanswered question on the presence, or not, of fusion hindrance.

Several attempts have been made over the past five decades to determine the $^{12}C+^{12}C$ reactions cross-sections [6,53,56–66]. However, the data still carry large uncertainties and show significant discrepancies between different data sets. Furthermore, no direct measurement has been possible at energies below $E_{c.m.} = 2.14$ MeV and indirect measurements [67] incited an intense debate [68,69]. For these reasons, further direct experimental investigations are required.

The low cross-sections make the direct measurement quite challenging. Further complications arise in the form of beam-induced background due to $^{1,2}H$ impurities present in the graphite targets that, through the $^{12}C+^{1,2}H$ reaction, having a considerably lower Coulomb barrier, hampered the $^{12}C+^{12}C$ cross-section determination. Previous experimen-

tal works have shown that said impurities can be reduced by heating the targets. This has been achieved in different ways: through resistances [60] or using intense beams to reach about 400–700 °C for 6–8 h [53,62]. While a reduction in H contamination was found in all cases, resulting in cleaner spectra, no systematic investigation was carried out to quantify this reduction or to assess the optimal conditions for low-energy measurements of the ^{12}C+^{12}C reactions cross-sections.

The ERNA Collaboration, using four GASTLY detectors at backward angles, optimized background identification and performed a quantitative study to asses depletion of hydrogen and deuterium impurities of carbon targets in situ (avoiding unnecessary air exposures) [31]. Measurements were conducted under controlled experimental conditions on natural graphite (NG) and HOPG targets of different purity, showing that deuterium (and hydrogen) content can be reduced by up to about 70–85% for HOPG and NG targets heated at temperatures above 1000 °C. A further reduction by a factor of 2.5 is achieved by enclosing the target chamber in a dry nitrogen environment (at a pressure slightly higher than the atmosphere) to minimise air leaks into the rest gas within the chamber. The detailed study can be found in [31]. Using the results from this study (intense beams for high target temperatures and a nitrogen atmosphere) to minimize target contamination, the ^{12}C+^{12}C reactions were measured and impurities could be identified and discarded from data.

The use of the GASTLY detectors in the measurement of the ^{12}C+^{12}C allowed for unambiguous identification of both protons and alfa particles, as can be seen in Figure 4, where it is shown a ΔE-E_{res} spectrum obtained with ^{12}C^{+3} beam with energy corresponding to $E_{c.m.}$ = 4.36 MeV. The spectrum refers to the detector placed at 121° (central angle) with respect to the beam axis, spanning an angular range from 113° to 132°. The IC section of the detector was using CF$_4$ at 35 mbar pressure.
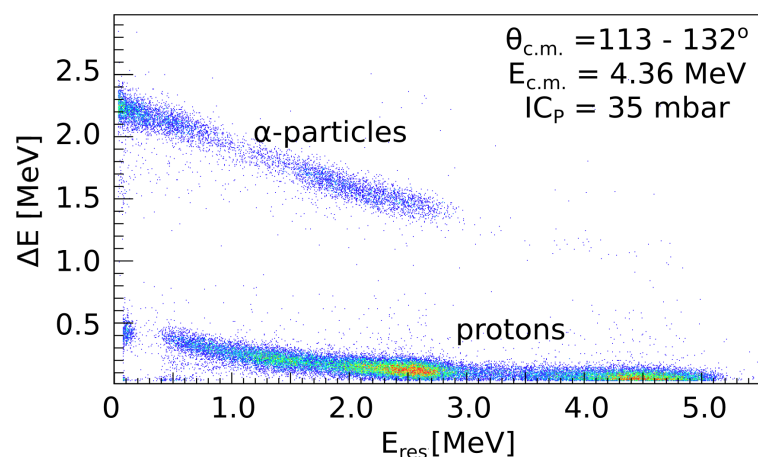

Figure 4. Sample ΔE-E_{res} spectrum obtained with a single detector at $E_{c.m.}$ = 4.36 MeV in the ^{12}C+^{12}C measurements campaign. The protons and α particles produced in the reactions are clearly identified. Adapted by permission from Springer Nature Customer Service Centre GmbH: Springer Nature, The European Physical Journal A - Hadrons and Nuclei, [30], Copyright (2018).

Similar spectra were obtained for all other beam energies. The thick target yield was obtained from the net number of proton events extracted and analyzed using only the E_{res} spectrum, once gated on the corresponding region of interest (ROI) in the ΔE-E_{res} matrix. The proton groups from p_0 up to p_6 could be identified, as well as the ^{12}C$(d,p)^{12}$C contribution allowing for a correct separation of the protons from each reaction.

4. Discussion

The measurement with ERNA of the 1323 and 1487 keV resonances' reaction yield in the ^{15}N$(\alpha, \gamma)^{19}$F reaction [5], leads to a better assessment of their widths. Indeed, the Γ_γ of both resonances were found in good agreement with literature values and Γ_α of

the 1487 keV resonance was found to be compatible with earlier determinations ([45] and references therein), while a significant difference was observed for the Γ_α of the 1323 keV resonance. However, the major result was the precision improvement on the Γ_α values, improved to about 5%.

Although the two measured resonances have energies so that they directly influence the reaction rate at a temperature of several GK, they also significantly influence the reaction rate at the AGB burning temperatures through their low energy tails, together with the direct capture component. In Figure 5, the reaction rate calculated according to [70], including the lower and upper uncertainty bands, 16th and 84th percentile, respectively, is shown as a ratio to the central value of [71]. The effect of the improved widths determination is clearly visible at temperature below 10^8 K, where the remaining uncertainty is dominated by the $E_{c.m.} = 364$ keV determination.
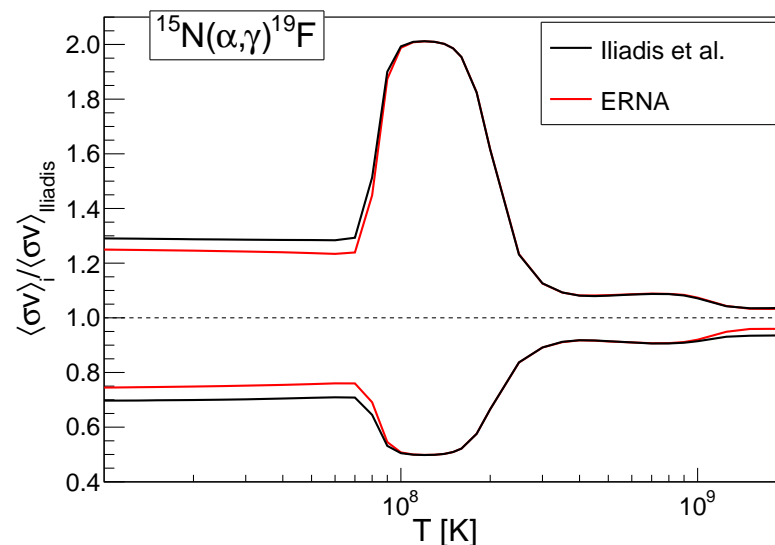

Figure 5. The lower and upper limits for the $^{15}N(\alpha, \gamma)^{19}F$ reaction rate are compared to the central value of Iliadis et al. [71]. The values of [71] are shown by the black curves, while the red curves correspond to the same calculation with updated values of the 1323 and 1487 keV resonance widths. The value of [71] are reprinted from Publication [71], Copyright (2010), with permission from Elsevier.

NG and HOPG targets 1 mm thick were studied using intense C beams to reach target temperatures of 200–1200 °C at the beam spot in order to minimize the target deuterium contaminants that could hamper the $^{12}C+^{12}C$ reactions. As a result, deuterium was reduced by 70–85% in natural graphite and HOPG targets (depending on detection angle). The scattering chamber was enclosed in a nitrogen atmosphere obtaining a further reduction by a factor 2.5 (see [31] for further details on target contaminants characterization). Such findings and improvements in the target deuterium contamination and their reduction open the possibility to expand the measurement range at lower energy. Along with this, the use of the GASTLY detector allows to perform reliable measurements up to $E_{c.m.} \simeq 2.3$ MeV.

5. Outlook

The ERNA RMS has proved to be a valuable tool in the measurement of the total cross-section of radiative capture reactions of astrophysical interest. In the present and near future, the experimental program aims at the extension of previous measurement campaigns, i.e., the low energy ranges of the $^{12}C(\alpha, \gamma)^{16}O$ and $^{15}N(\alpha, \gamma)^{19}F$ cross-section, and of the $^{7}Be(p, \gamma)^{8}B$ at around $E_{c.m.} \sim 1$ MeV.

The more recent activity with the GASTLY array has also given promising results on the $^{12}C+^{12}C$ fusion process and the ERNA Collaboration continues working toward the measurement of the $^{12}C+^{12}C$ fusion process in the astrophysical energy range with the aim of confirming or rejecting the existence of resonances within the Gamow energy

window. Using a partial configuration available in the first development phase of the GASTLY detector array, i.e., four GASTLY detectors with the SSD as an entire pad, the thick target yield has been measured in the energy range $E_{c.m.}$ = 2.51 – 4.36 MeV and the astrophysical S-factors of $^{12}C(^{12}C,p)^{23}Na$ and $^{12}C(^{12}C,\alpha)^{20}Ne$ have been extracted. Results will be presented in a forthcoming publication.

Charged particle spectroscopy measurements will continue with the investigation of the $^{12}C+^{16}O$ fusion process. In addition, owing to the good performances of the GASTLY array in terms of particle identification, several other reactions can be envisioned in the longer term.

References

1. Rolfs, C.E.; Rodney, W.S. *Cauldrons in the Cosmos: Nuclear Astrophysics*; The University of Chicago Press: Chicago, IL, USA, 1988.
2. Rolfs, C.; Barnes, C. Radiative Capture Reactions in Nuclear Astrophysics. *Annu. Rev. Nucl. Part. Sci.* **1990**, *40*, 45–78. [CrossRef]
3. Brune, C.R.; Davids, B. Radiative Capture Reactions in Astrophysics. *Annu. Rev. Nucl. Part. Sci.* **2015**, *65*, 87–112. [CrossRef]
4. Di Leva, A.; De Cesare, M.; Schürmann, D.; De Cesare, N.; D'Onofrio, A.; Gialanella, L.; Kunz, R.; Imbriani, G.; Ordine, A.; Roca, V.; et al. Recoil separator ERNA: Measurement of $^3He(\alpha,\gamma)^7Be$. *Nucl. Instr. Meth. A* **2008**, *595*, 381–390. [CrossRef]
5. Di Leva, A.; Imbriani, G.; Buompane, R.; Gialanella, L.; Best, A.; Cristallo, S.; De Cesare, M.; D'Onofrio, A.; Duarte, J.G.; Gasques, L.R.; et al. Measurement of 1323 and 1487 keV resonances in $^{15}N(\alpha,\gamma)^{19}F$ with the recoil separator ERNA. *Phys. Rev. C* **2017**, *95*, 045803. [CrossRef]
6. Zickefoose, J.; Leva, A.D.; Strieder, F.; Gialanella, L.; Imbriani, G.; Cesare, N.D.; Rolfs, C.; Schweitzer, J.; Spillane, T.; Straniero, O.; et al. Measurement of the $^{12}C(^{12}C,p)^{23}Na$ cross section near the Gamow energy. *Phys. Rev. C* **2018**, *97*, 065806. [CrossRef]
7. Terrasi, F.; Marzaioli, F.; Buompane, R.; Passariello, I.; Porzio, G.; Capano, M.; Helama, S.; Oinonen, M.; Nöjd, P.; Uusitalo, J.; et al. Can the ^{14}C Production in 1055 CE be Affected by SN1054? *Radiocarbon* **2020**, *62*, 1403–1418. [CrossRef]
8. Brandi, F.; Labate, L.; Rapagnani, D.; Buompane, R.; Leva, A.d.; Gialanella, L.; Gizzi, L.A. Optical and spectroscopic study of a supersonic flowing helium plasma: Energy transport in the afterglow. *Sci. Rep.* **2020**, *10*, 5087. [CrossRef]
9. Buompane, R.; Di Leva, A.; Gialanella, L.; D'Onofrio, A.; De Cesare, M.; Duarte, J.G.; Fülöp, Z.; Gasques, L.R.; Gyürky, G.; Morales-Gallegos, L.; et al. Determination of the $^7Be(p,\gamma)^8B$ cross section at astrophysical energies using a radioactive ^7Be ion beam. *Phys. Lett. B* **2021**, *824*, 136819. [CrossRef]
10. Santonastaso, C.; Buompane, R.; Di Leva, A.; Morales-Gallegos, L.; Itaco, N.; Landi, G.; Neitzert, H.; Rapagnani, D.; Gialanella, L. Change in the ^7Be half-life in different environments. *Nuovo Cimento* **2021**, *100*, 44.
11. Ruiz, C.; Greife, U.; Hager, U. Recoil separators for radiative capture using radioactive ion beams. *Eur. Phys. J. A* **2014**, *50*, 99. [CrossRef]
12. Schürmann, D.; Strieder, F.; Di Leva, A.; Gialanella, L.; De Cesare, N.; D'Onofrio, A.; Imbriani, G.; Klug, J.; Lubritto, C.; Ordine, A.; et al. Recoil separator ERNA: Charge state distribution, target density, beam heating, and longitudinal acceptance. *Nucl. Instr. Meth. A* **2004**, *531*, 428–434. [CrossRef]
13. Gialanella, L.; Strieder, F.; Brand, K.; Campajola, L.; D'Onofrio, A.; Greife, U.; Huttel, E.; Petrazzuolo, F.; Roca, V.; Rolfs, C.; et al. A recoil separator for the measurement of radiative capture reactions. *Nucl. Instr. Meth. A* **1996**, *376*, 174–184. [CrossRef]
14. Rogalla, D.; Theis, S.; Campajola, L.; D'Onofrio, A.; Gialanella, L.; Greife, U.; Imbriani, G.; Ordine, A.; Roca, V.; Rolfs, C.; et al. Recoil separator ERNA: Ion beam purification. *Nucl. Instr. Meth. A* **1999**, *437*, 266–273. [CrossRef]
15. Gialanella, L.; Strieder, F.; Campajola, L.; D'Onofrio, A.; Greife, U.; Gyurky, G.; Imbriani, G.; Oliviero, G.; Ordine, A.; Roca, V.; et al. Absolute cross section of p($^7Be,\gamma)^8B$ using a novel approach. *Eur. Phys. J. A* **2000**, *7*, 303–305. [CrossRef]

16. Rogalla, D.; Schürmann, D.; Strieder, F.; Aliotta, M.; DeCesare, N.; DiLeva, A.; Lubritto, C.; D'Onofrio, A.; Gialanella, L.; Imbriani, G.; et al. Recoil separator ERNA: Acceptances in angle and energy. *Nucl. Instr. Meth. A* **2003**, *513*, 573–578. [CrossRef]

17. Gialanella, L.; Schürmann, D.; Strieder, F.; Di Leva, A.; De Cesare, N.; D'Onofrio, A.; Imbriani, G.; Klug, J.; Lubritto, C.; Ordine, A.; et al. Recoil separator ERNA: Gas target and beam suppression. *Nucl. Instr. Meth. A* **2004**, *522*, 432–438. [CrossRef]

18. deBoer, R.J.; Görres, J.; Wiescher, M.; Azuma, R.E.; Best, A.; Brune, C.R.; Fields, C.E.; Jones, S.; Pignatari, M.; Sayre, D.; et al. The ^{12}C$(\alpha, \gamma)^{16}$O reaction and its implications for stellar helium burning. *Rev. Mod. Phys.* **2017**, *89*, 035007. [CrossRef]

19. Smith, M.S.; Blackmon, J.C.; Koehler, P.E.; Lewis, T.A.; McConnell, J.W.; Milner, W.T.; Pierce, D.E.; Shapira, D.; Bardayan, D.W.; Chen, A.A.; et al. Commissioning of the Daresbury recoil seperator for nuclear astrophysics measurements at the Holifield radioactive ion beam facility. In *Stellar Evolution, Stellar Explosions and Galactic Chemical Evolution, Proceedings of the 2nd Oak Ridge Symposium on Atomic and Nuclear Astrophysics, Oak Ridge, Tennessee, 2–6 December 1997*; Mezzacappa, A., Ed.; IOP Publishing Ltd.: Bristol, UK, 1998; p. 511, ISBN:9780750305556.

20. Hutcheon, D.A.; Bishop, S.; Buchmann, L.; Chatterjee, M.L.; Chen, A.A.; D'Auria, J.M.; Engel, S.; Gigliotti, D.; Greife, U.; Hunter, D.; et al. The DRAGON facility for nuclear astrophysics at TRIUMF-ISAC: Design, construction and operation. *Nucl. Instr. Meth. A* **2003**, *498*, 190–210. [CrossRef]

21. Couder, M.; Angulo, C.; Galster, W.; Graulich, J.S.; Leleux, P.; Lipnik, P.; Tabacaru, G.; Vanderbist, F. Performance of the ARES recoil separator for (p,γ) reaction measurements. *Nucl. Instr. Meth. A* **2003**, *506*, 26–34. [CrossRef]

22. Ikeda, N.; Sagara, K.; Tsuruta, K.; Oba, H.; Ohta, T.; Noguchi, Y.; Ichikawa, K.; Miwa, Y.; Morinobu, S. Facilities for direct measurement of ^{12}C$(\alpha, \gamma)^{16}$O reaction cross section at KUTL. *Nucl. Phys. A* **2003**, *718*, 558. [CrossRef]

23. Meisel, Z.; Moran, M.; Gilardy, G.; Schmitt, J.; Seymour, C.; Couder, M. Energy acceptance of the St. George recoil separator. *Nucl. Instr. Meth. A* **2017**, *850*, 48–53. [CrossRef]

24. Miskovich, S.A. Commissioning of the Separator for Capture Reactions in Astrophysics. Ph.D. Thesis, Michigan State University, East Lansing, MI, USA 2021.

25. Terrasi, F.; Rogalla, D.; De Cesare, N.; D'Onofrio, A.; Lubritto, C.; Marzaioli, F.; Passariello, I.; Rubino, M.; Sabbarese, C.; Casa, G.; et al. A new AMS facility in Caserta/Italy. *Nucl. Instr. Meth. B* **2007**, *259*, 14–17. [CrossRef]

26. Gialanella, L.; Greife, U.; De Cesare, N.; D'Onofrio, A.; Romano, M.; Campajola, L.; Formicola, A.; Fulop, Z.; Gyurky, G.; Imbriani, G.; et al. Off-line production of a ^{7}Be radioactive ion beam. *Nucl. Instr. Meth. B* **2002**, *197*, 150–154. [CrossRef]

27. Limata, B.N.; Gialanella, L.; Leva, A.D.; Cesare, N.D.; D'Onofrio, A.; Gyurky, G.; Rolfs, C.; Romano, M.; Rogalla, D.; Rossi, C.; et al. ^{7}Be radioactive beam production at CIRCE and its utilization in basic and applied physics. *Nucl. Instr. Meth. B* **2008**, *266*, 2117–2121. [CrossRef]

28. Schürmann, D.; Di Leva, A.; Gialanella, L.; De Cesare, M.; De Cesare, N.; Imbriani, G.; D'Onofrio, A.; Romano, M.; Romoli, M.; Terrasi, F. A windowless hydrogen gas target for the measurement of ^{7}Be(p, γ)^{8}B with the recoil separator ERNA. *Eur. Phys. J. A* **2013**, *49*, 80. [CrossRef]

29. Rapagnani, D.; Buompane, R.; Di Leva, A.; Gialanella, L.; Busso, M.; De Cesare, M.; De Stefano, G.; Duarte, J.; Gasques, L.; Morales-Gallegos, L.; et al. A supersonic jet target for the cross section measurement of the ^{12}C$(\alpha, \gamma)^{16}$O reaction with the recoil mass separator ERNA. *Nucl. Instr. Meth. B* **2017**, *407*, 217–221. [CrossRef]

30. Romoli, M.; Morales-Gallegos, L.; Aliotta, M.; Bruno, C.G.; Buompane, R.; D'Onofrio, A.; Davinson, T.; De Cesare, M.; Di Leva, A.; Di Meo, P.; et al. Development of a two-stage detection array for low-energy light charged particles in nuclear astrophysics applications. *Eur. Phys. J. A* **2018**, *54*, 142. [CrossRef]

31. Morales-Gallegos, L.; Aliotta, M.; Bruno, C.; Buompane, R.; Davinson, T.; De Cesare, M.; Di Leva, A.; D'Onofrio, A.; Duarte, J.; Gasques, L.; et al. Reduction of deuterium content in carbon targets for ^{12}C+^{12}C reaction studies of astrophysical interest. *Eur. Phys. J. A* **2018**, *54*. [CrossRef]

32. Brune, C.R.; Sayre, D.B. Energy deconvolution of cross-section measurements with an application to the ^{12}C$(\alpha, \gamma)^{16}$O reaction. *Nucl. Instr. Meth. A* **2013**, *698*, 49–59. [CrossRef]

33. Iliadis, C. *Nuclear Physics of Stars*; WILEY-VCH Verlag GmbH & Co. KGaA, Weinheim: Berlin, Germany, 2007.

34. Schürmann, D.; Di Leva, A.; Gialanella, L.; Rogalla, D.; Strieder, F.; De Cesare, N.; D'Onofrio, A.; Imbriani, G.; Kunz, R.; Lubritto, C.; et al. First direct measurement of the total cross-section of ^{12}C$(\alpha, \gamma)^{16}$O. *Eur. Phys. J. A* **2005**, *26*, 301–305. [CrossRef]

35. Matei, C.; Buchmann, L.; Hannes, W.R.; Hutcheon, D.A.; Ruiz, C.; Brune, C.R.; Caggiano, J.; Chen, A.A.; D'Auria, J.; Laird, A.; et al. Measurement of the Cascade Transition via the First Excited State of ^{16}O in the ^{12}C$(\alpha, \gamma)^{16}$O Reaction, and Its S Factor in Stellar Helium Burning. *Phis. Rev. Lett.* **2006**, *97*, 242503. [CrossRef] [PubMed]

36. Schürmann, D.; Di Leva, A.; Gialanella, L.; Kunz, R.; Strieder, F.; De Cesare, N.; De Cesare, M.; D'Onofrio, A.; Fortak, K.; Imbriani, G.; et al. Study of the 6.05 MeV cascade transition in ^{12}C$(\alpha, \gamma)^{16}$O. *Phys. Lett. B* **2011**, *703*, 557–561. [CrossRef]

37. Buompane, R.; De Cesare, N.; Di Leva, A.; D'Onofrio, A.; Gialanella, L.; Romano, M.; De Cesare, M.; Duarte, J.G.; Fülöp, Z.; Morales-Gallegos, L.; et al. Test measurement of ^{7}Be(p, γ)^{8}B with the recoil mass separator ERNA. *Eur. Phys. J. A* **2018**, *54*, 92. [CrossRef]

38. Cristallo, S.; Di Leva, A.; Imbriani, G.; Piersanti, L.; Abia, C.; Gialanella, L.; Straniero, O. Effects of nuclear cross sections on ^{19}F nucleosynthesis at low metallicities. *Astron. Astroph.* **2014**, *570*, A46. [CrossRef]

39. Forestini, M.; Goriely, S.; Jorissen, A.; Arnould, M. Fluorine production in thermal pulses on the asymptotic giant branch. *Astron. Astrophys.* **1992**, *261*, 157.

40. Abia, C.; Recio-Blanco, A.; de Laverny, P.; Cristallo, S.; Domínguez, I.; Straniero, O. Fluorine in Asymptotic Giant Branch Carbon Stars Revisited. *Astrophys. J.* **2009**, *694*, 971–977. [CrossRef]

41. Woosley. Supernova neutrinos, neutral currents and the origin of fluorine. *Nature* **1988**, *334*, 45–47. [CrossRef]

42. Meynet, G.; Arnould, M. Synthesis of ^{19}F in Wolf-Rayet stars. *Astron. Astrophys.* **2000**, *335*, 176–180.

43. Straniero, O.; Gallino, R.; Busso, M.; Chiefei, A.; Raiteri, C.M.; Limongi, M.; Salaris, M. Radiative ^{13}C Burning in Asymptotic Giant Branch Stars and s-Processing. *Astrophys. J. Lett.* **1995**, *440*, L85. [CrossRef]

44. Gallino, R.; Arlandini, C.; Busso, M.; Lugaro, M.; Travaglio, C.; Straniero, O.; Chieffi, A.; Limongi, M. Evolution and Nucleosynthesis in Low-Mass Asymptotic Giant Branch Stars. II. Neutron Capture and the S-Process. *Astrophys. J.* **1998**, *497*, 388–403. [CrossRef]

45. Wilmes, S.; Wilmes, V.; Staudt, G.; Mohr, P.; Hammer, J.W. The ^{15}N$(\alpha,\gamma)^{19}$F reaction and nucleosynthesis of ^{19}F. *Phys. Rev. C* **2002**, *66*, 065802. [CrossRef]

46. Rogers, D.W.O.; Beukens, R.P.; Diamond, W.T. Resonances in the ^{15}N$(\alpha, \gamma)^{19}$F Reaction Between $E_\alpha = 1.68$ and 2.72 MeV. *Can. J. Phys.* **1972**, *50*, 2428–2443. [CrossRef]

47. Price, P.C. The Radiative Capture of Alpha Particles in ^{15}N. *Proc. Phys. Society. Sect. A* **1957**, *70*, 661–667. [CrossRef]

48. de Oliveira, F.; Coc, A.; Aguer, P.; Angulo, C.; Bogaert, G.; Kiener, J.; Lefebvre, A.; Tatischeff, V.; Thibaud, J.P.; Fortier, S.; et al. Determination of α-widths in $[19]$F relevant to fluorine nucleosynthesis. *Nucl. Phys. A* **1996**, *597*, 231–252. [CrossRef]

49. Di Leva, A.; Pezzella, A.; De Cesare, N.; D'Onofrio, A.; Gialanella, L.; Romano, M.; Romoli, M.; Schürmann, D.; Terrasi, F.; Imbriani, G. ^{14,15}N beam from cyanide compounds. *Nucl. Instr. Meth. A* **2012**, *689*, 98–101. [CrossRef]

50. Straniero, O.; Piersanti, L.; Cristallo, S. Do we really know M_{up} (i.e., the transition mass between Type Ia and core-collapse supernova progenitors)? *J. Phys. Conf. Ser. (NPA6)* **2016**, *665*, 012008. [CrossRef]

51. Tang, X.; Bucher, B.; Fang, X.; Notani, M.; Tan, W.P.; Li, Y.; Mooney, P.; Esbensen, H.; Jiang, C.L.; Rehm, K.E.; et al. How does the carbon fusion reaction happen in stars? *Nucl. Phys. At. Energy* **2013**, *14*, 224–232. [CrossRef]

52. Strieder, F.; Rolfs, C. Reaction data for light element nucleosynthesis. *Prog. Part. Nucl. Phys.* **2007**, *59*, 562–578. [CrossRef]

53. Barrón-Palos, L.; Aguilera, E.F.; Aspiazu, J.; Huerta, A.; Martínez-Quiroz, E.; Monroy, R.; Moreno, E.; Murillo, G.; Ortíz, M.E.; Policroniades, R.; et al. Absolute cross sections measurement for the ^{12}C+^{12}C system at astrophysically relevant energies. *Nucl. Phys. A* **2006**, *779*, 318–332. [CrossRef]

54. Angulo, C. Experimental Tools for Nuclear Astrophysics. *Lect. Notes Phys.* **2009**, *764*, 253–282.

55. Jiang, C.L.; Back, B.B.; Esbensen, H.; Janssens, R.F.; Rehm, K.E.; Charity, R.J. Origin and Consequences of ^{12}C+^{12}C Fusion Resonances at Deep Sub-barrier Energies. *Phys. Rev. Lett.* **2013**, *110*, 072701. [CrossRef] [PubMed]

56. Patterson, J.R.; Winkler, H.; Zaidins, C.S. Experimental investigation of the stellar nuclear reaction ^{12}C+^{12}C at low energies. *Astrophys. J.* **1969**, *157*, 367–373. [CrossRef]

57. Mazarakis, M.G.; Stephens, W.E. Experimental Measurements of the ^{12}C+^{12}C Nuclear Reactions at Low Energies. *Phys. Rev. C* **1973**, *7*. [CrossRef]

58. Becker, H.W.; Kettner, K.U.; Rolfs, C.; Trautvetter, H.P. The ^{12}C+^{12}C Reaction at Subcoulomb Energies (II). *Z. Phys. A* **1981**, *303*, 305–312. [CrossRef]

59. High, M.D.; Cûjec, B. The ^{12}C+^{12}C sub-coulomb fusion cross section. *Nucl. Phys. A* **1977**, *282*, 181–188. [CrossRef]

60. Kettner, K.U.; Lorenz-Wirzba, H.; Rolfs, C. The ^{12}C+^{12}C reaction at subcoulomb energies (I). *Z. Phys. A* **1980**, *298*, 65–75. [CrossRef]

61. Rosales, P.; Aguilera, E.F.; Martinez-Quiroz, E.; Murillo, G.; Policroniades, R.; Varela, A.; Moreno, E.; Fernández, M.; Berdejo, H.; Aspiazu1, J.; et al. Sub-Coulomb fusion excitation function for ^{12}C+^{12}C. *Rev. Mex. De Fis. S4* **2003**, *49*, 88–91.

62. Aguilera, E.F.; Rosales, P.; Martinez-Quiroz, E.; Murillo, G.; Fernández, M.; Berdejo, H.; Lizcano, D.; Gómez-Camacho, A.; Policroniades, R.; Varela, A.; et al. New γ-ray measurements for ^{12}C+^{12}C sub-Coulomb fusion: Toward data unification. *Phys. Rev. C* **2006**, *73*, 064601. [CrossRef]

63. Spillane, T.; Raiola, F.; Rolfs, C.; Schürmann, D.; Strieder, F.; Zeng, S.; Becker, H.W.; Bordeanu, C.; Gialanella, L.; Romano, M.; et al. ^{12}C+^{12}C Fusion Reactions near the Gamow Energy. *Phys. Rev. Lett.* **2007**, *98*, 122501. [CrossRef]

64. Jiang, C.L.; Santiago-Gonzalez, D.; Almaraz-Calderon, S.; Rehm, K.E.; Back, B.B.; Auranen, K.; Avila, M.L.; Ayangeakaa, A.D.; Bottoni, S.; Carpenter, M.P.; et al. Reaction rate for carbon burning in massive stars. *Phys. Rev. C* **2018**, *97*, 012801. [CrossRef]

65. Fruet, G.; Courtin, S.; Heine, M.; Jenkins, D.G.; Adsley, P.; Brown, A.; Canavan, R.; Catford, W.N.; Charon, E.; Curien, D.; et al. Advances in the Direct Study of Carbon Burning in Massive Stars. *Phys. Rev. Lett.* **2020**, *124*, 192701. [CrossRef] [PubMed]

66. Tan, W.P.; Boeltzig, A.; Dulal, C.; deBoer, R.J.; Frentz, B.; Henderson, S.; Howard, K.B.; Kelmar, R.; Kolata, J.J.; Long, J.; et al. New Measurement of ^{12}C+^{12}C Fusion Reaction at Astrophysical Energies. *Phys. Rev. Lett.* **2020**, *124*, 192702. [CrossRef]

67. Tumino, A.; Spitaleri, C.; Cognata, M.L.; Cherubini, S.; Guardo, G.L.; Gulino, M.; Hayakawa, S.; Indelicato, I.; Lamia, L.; Petrascu, H.; et al. An increase in the ^{12}C+^{12}C fusion rate from resonances at astrophysical energies. *Nature* **2018**, *557*, 687–690. [CrossRef] [PubMed]

68. Mukhamedzhanov, A.M.; Pang, D.Y. Astrophysical factors of ^{12}C+^{12}C fusion from Trojan horse method. *Phys. Rev. C* **2019**, *99*, 064618. [CrossRef]

69. Tumino, A.; Spitaleri, C.; Cognata, M.L.; Cherubini, S.; Guardo, G.L.; Gulino, M.; Hayakawa, S.; Indelicato, I.; Lamia, L.; Petrascu, H.; et al. Reply to the Comments on the ^{12}C+^{12}C fusion S^*-factor. *arXiv* **2018**, arXiv:1807.06148.

70. Longland, R.; Iliadis, C.; Champagne, A.E.; Newton, J.R.; Ugalde, C.; Coc, A.; Fitzgerald, R. Charged-particle thermonuclear reaction rates: I. Monte Carlo method and statistical distributions. *Nucl. Phys. A* **2010**, *841*, 1–30. [CrossRef]
71. Iliadis, C.; Longland, R.; Champagne, A.E.; Coc, A.; Fitzgerald, R. Charged-particle thermonuclear reaction rates: II. Tables and graphs of reaction rates and probability density functions. *Nucl. Phys. A* **2010**, *841*, 31–250. [CrossRef]